Electron acceleration in sub-relativistic wakefields driven by few-cycle laser pulses

B Beaurepaire, Agustin Lifschitz, Jérôme Faure

Electron acceleration in sub-relativistic wakefields driven by few-cycle laser pulses

B. Beaurepaire, A. Lifschitz, and J. Faure
Laboratoire d'Optique Appliquée,
ENSTA-CNRS-Ecole Polytechnique,
UMR 7639, 91761 Palaiseau, France

Abstract

Using Particle-in-Cell simulations, we study the interaction of few mJ-few cycle laser pulses with an underdense plasma at resonant density. In this previously unexplored regime, it is found that group velocity dispersion is a key ingredient of the interaction. The concomitant effects of dispersion and plasma nonlinearities causes a deceleration of the wakefield phase velocity, which becomes sub-relativistic. Electron injection in this sub-relativistic wakefield is enhanced and leads to the production of a femtosecond electron bunch with picocoulomb of charge in the 5-10 MeV energy range. Such an electron bunch is of great interest for application to ultrafast electron diffraction. In addition, in this dispersion dominated regime, it is shown that positively chirped laser pulses can be used as a tuning knob for compensating plasma dispersion, increasing the laser amplitude during self-focusing and optimizing the trapped charge.

I. INTRODUCTION

Recent advances in laser technology have enabled the development of high repetition rate kHz laser systems delivering pulses with only a few optical cycles [1]. The main application of such pulses has been high harmonic generation in gases at modest intensity ($I \simeq 10^{14}\,\mathrm{W/cm^2}$) and attosecond pulse generation [2]. Recently, 5 fs laser pulses at the multimillijoule level have become available [3, 4] and intensities in excess of $10^{18}\,\mathrm{W/cm^2}$ are becoming accessible with these compact kHz laser systems. These progress have permitted to perform high intensity laser plasma interaction experiments at kHz repetition rate and hold the promise of high repetition secondary sources from laser plasma interaction. To date, experiments have mostly been performed on solid targets for electron generation [5] or high harmonic generation [6, 7] but little attention was given to underdense laser plasma interaction and laser wakefield acceleration. However, with the current laser parameters, laser wakefield acceleration of electrons at kHz repetition rate is within reach.

Currently, most laser wakefield experiments are performed with joule level laser systems and electrons are accelerated in the 100 MeV -1 GeV range [8, 9]. However, scaling laws [10, 11] indicate that a 5 fs-5 mJ laser would be able to produce femtosecond electron bunches at 5-10 MeV. Such an electron beam would be of great interest for probing matter in ultrafast electron diffraction experiments (UED) [12]. Indeed, laser wakefield accelerators can provide electron bunches with femtosecond durations [13] which are well-synchronized with the driving laser in a jitter free fashion. Recently, a first proof-of-principle experiment has shown that a few millijoule kHz system could be used to drive a laser wakefield accelerator and produce 100 keV electron beams [14]. After filtering and transport, this electron beam was used to produce clear diffraction patterns on an aluminum thin film [15]. In Ref. [15], the electron kinetic energy was limited to 100 keV because the experiment did not operate in the blowout regime. In recent years, first attempts to reach the blowout regime with mJ laser systems have been performed. By using a 8 fs and 40 mJ laser pulse, electrons bunches of energy > 20 MeV have been produced [16]. The electron energy was too high for a practical application in UED. In this context, the next challenge is to bring electron acceleration at kHz repetition rate using about 10 times less laser energy with shorter pulses composed of nearly a single cycle and targeting electron energies of 3-10 MeV, a range suitable for performing electron diffraction [17–19].

This paper presents a numerical investigation, by means of Particle-In-Cell (PIC) simulations, of the interaction of few-cycle laser pulses at the mJ level with an underdense plasma, with the goal of downscaling a laser wakefield accelerator to the MeV energy range. These few-cycle laser pulses are rather exotic for laser-plasma interaction: (i) the usual averaging of the ponderomotive force over the optical cycle is no longer valid, (ii) the carrier envelope phase (CEP) starts to matter [20], (iii) group velocity dispersion (GVD) in the plasma can no longer be neglected. In this paper, we show that the dynamics of electron trapping and acceleration is mainly determined by the fast and dramatic evolution of the pulse temporal profile and spectrum due to the complex interplay of GVD and nonlinear effects. The concomitant effects of dispersion and plasma nonlinearities causes a deceleration of the wakefield phase velocity, which becomes sub-relativistic. Electron trapping in this sub-relativistic wakefield is enhanced and leads to a massive injection of electrons. This is in contrast with the classical picture, valid for longer pulses, in which the smooth evolution of the laser pulse under self-focusing and self-steepening determine the physics of injection and acceleration. Finally, our study confirms the scaling laws of Ref. [10] and shows that by choosing the right parameters, pC of charge in the MeV range can be produced using only few millijoule few-cycle laser pulses. The paper is organized as follows: section II is an overview of the basic mechanisms such as nonlinear effects and dispersion. Section III presents the

results of PIC simulations showing the trapping of electrons in sub-relativistic wakefields. Finally, section IV points out that in this dispersion dominated regime, the laser chirp has large effects and can be used to optimize and tune the interaction.

II. BASIC PHYSICAL MECHANISMS: DISPERSION AND NONLINEAR EFFECTS

In order to introduce the basic phenomena, we follow the simplified description of Ref. [21]. The refractive index of an underdense plasma in which a linearly polarized laser pulse propagates is given by:

$$\eta = 1 - \frac{1}{2}\frac{\omega_p^2}{\omega_0^2}\left(1 + \frac{\delta n}{n} - \frac{\langle a\rangle^2}{2} - 2\frac{\delta\omega}{\omega_0}\right) \qquad (1)$$

where ω_0 is the laser central frequency, $\omega_p = \sqrt{ne^2/m_e\epsilon_0}$ the plasma frequency (n is the electron density, e and m_e are the electron charge and mass), δn is the perturbation to the electronic density due to plasma waves and $\langle a\rangle$ is the normalized vector potential averaged over an optical cycle. The first term represents the perturbation due to the plasma wave, the second one represents the perturbation due to relativistic nonlinearities and the third one modulations of the index of refraction due to the spectral bandwidth $\delta\omega/\omega_0$, i.e. it is the term responsible for GVD. Note that this expression results from a linear development and is only valid in the weakly relativistic regime, $a^2 \ll 1$, in tenuous plasmas $\omega_p/\omega_0 \ll 1$, and for long enough pulses so that the envelop approximation is valid: $\omega_0\Delta t \gg 1$, i.e. it is not valid for few-cycle laser pulses. However, it will suffice for our heuristic discussion. Equation 1 is the basis for understanding various nonlinearities such as relativistic self-focussing [22, 23], self-modulation [24–26], self-steepening [27, 28] or self-compression [29, 30].

In the short pulse limit (i.e. $\Delta t \lesssim \lambda_p$), the first two terms can explain spectral broadening as well as the self-compression that occurs during the interaction. Spectral broadening originates from local changes of the index of refraction: $\delta\omega_0/\omega_0 \propto -\partial\eta/\partial\zeta$, where $\zeta = x - v_g t$ is the moving frame coordinate along the propagation axis x, and v_g is the laser group velocity. In equation 1, the term $-\langle a\rangle^2/2$ is responsible for relativistic self phase modulation (SPM) which cause the front (rear) of the pulse to be red-shifted (blue-shifted). This effect causes a symmetric broadening of the spectrum. The term $\delta n/n$ is responsible for local frequency changes due to the plasma waves, and causes the frequency to decrease in regions where the refractive index gradient is negative. This results in asymmetric broadening of the spectrum and in the case of laser pulses that are sufficiently short compared to λ_p it mainly causes a red shift of the laser central frequency. Both red shifting and spectral broadening have been observed experimentally [31, 32]. Thus, the combined effect of the plasma wakefield and SPM typically results in red shifting at the front of the pulse and blue shifting at the rear. The varying group velocity along the plasma wave can then cause the self-compression of the pulse which can reach durations shorter than the initial transform limit, as measured in Ref. [31] and [32]. Note that these nonlinear effects can also be described in the framework of photon kinetic theory, in which redshifting (blueshifting) is also referred to as photon deceleration (acceleration) [33, 34].

Most experiments operate in the nonlinear regime where $a^2 > 1$ and $\delta n/n \sim 1$. In addition, pulse durations are usually greater than 30 fs, so that $\delta\omega_0/\omega_0 < 0.1$. Thus, in state-of-the-art experiments, the effect of dispersion is usually discarded because it can be neglected compared to nonlinear effects. On the contrary, with few-cycle laser pulses, the bandwidth is very broad: $\delta\omega_0/\omega_0 \sim 1/4$ for 5 fs pulse at 800 nm and dispersion can no longer be neglected.

In the linear theory of dispersion of plasmas (see Appendix), an ultrashort pulse stretches as it propagates according to $\Delta t(x) = \Delta t_0(1 + x^2/L_p^2)^{1/2}$, where Δt_0 and Δt are respectively the r.m.s. transform limited duration and the chirped duration. Here L_p is the characteristic plasma length over which the pulse duration changes. L_p is given formally by

$$L_p = \frac{2c\Delta t_0}{\omega_p^2}\left\langle\left(\frac{1}{\omega^2} - \left\langle\frac{1}{\omega^2}\right\rangle\right)^2\right\rangle^{-1/2} \qquad (2)$$

where $\langle\ \rangle$ represents the average over the intensity distribution. This expression is valid for arbitrary broadband pulses and includes only the second order dispersion term. A somewhat more compact expression for L_p can be obtained assuming a narrow bandwidth $\delta\omega \ll \omega_0$, although this is not strictly valid for few-cycle laser pulses. The result gives

$$L_p = 2c\Delta t_0^2\frac{\omega_0^3}{\omega_p^2} \qquad (3)$$

This expression clearly shows that GVD increases greatly with laser bandwidth, plasma density and also for longer laser wavelengths: $L_p \propto \lambda_0^{-3}$. According to this analytical study, the duration of a 5 fs transform limited pulse is increased by a factor $\sqrt{2}$ after propagating only 111 µm in a homogeneous plasma electronic density $8.7\times10^{19}\mathrm{cm}^{-3}$. After some propagation in the plasma ($x > 0$), the laser pulse becomes negatively chirped, with the high frequencies at the front of the pulse and the low frequencies at the rear. This chirp manifests itself in Fourier space by examining the phase of the field $E(\omega) = |E(\omega)|\exp[i\phi(\omega)]$. For a negative chirp, the spectral phase $\phi(\omega)$ has a negative quadratic behavior. In the next section, we will study on the next section the effect of dispersion and nonlinearities in full 3D PIC simulations.

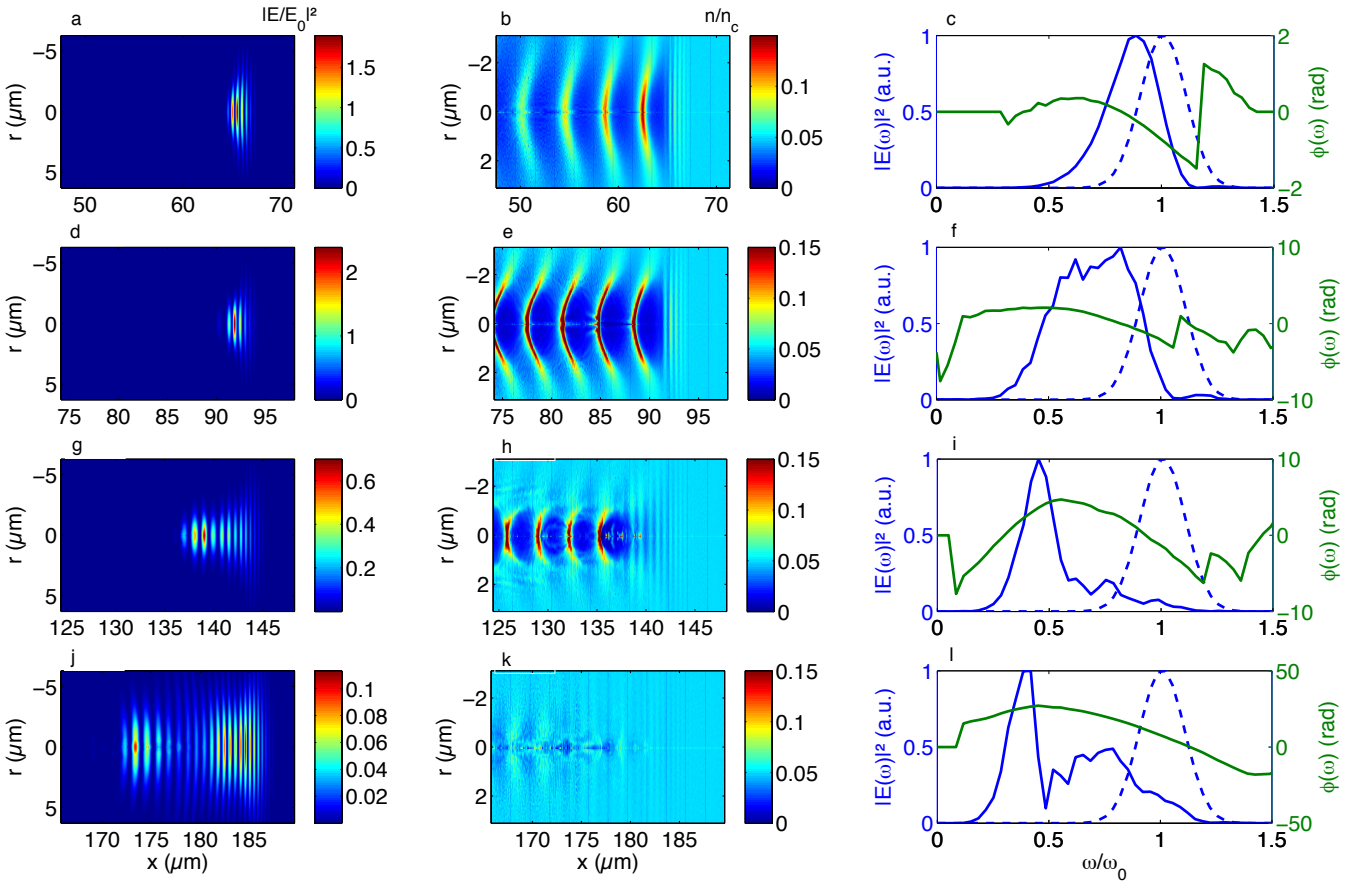

FIG. 1: Propagation of a 5 fs laser pulse. a) - d) - g) - j) snapshots of the laser field $|E/E_0|^2$ at various positions along propagation. b) - e) - h)- k) corresponding electron density n/n_c showing wakefield excitation. c) - f) - i) - l) corresponding on-axis laser spectrum (full blue line) and spectral phase (full green line); the dashed blue line represents the initial laser spectrum.

III. PIC SIMULATIONS OF THE PROPAGATION OF FEW-CYCLE 5 FS LASER PULSES

We have simulated laser-plasma interaction using the fully electromagnetic PIC code Calder-Circ [35]. We ran simulations with realistic experimental parameters, namely a 5 fs Full Width at Half Maximum(FWHM) pulse centered around $\lambda_0 = 800$ nm and with an energy of 4.1 mJ. The pulse is propagating in an underdense plasma, whose longitudinal density profile consists of a 203 μm plateau preceded and followed by a 63 μm ramp. The electronic density on the plateau is $n = 0.05 \times n_c = 8.7 \times 10^{19} cm^{-3}$. By focusing this laser beam at the beginning of the plateau, down to a waist of 4.3 μm, the laser intensity is I = 2.6x10^{18} W/cm^{-2}. The corresponding values of the normalized vector potential and laser power are respectively $a_0 = 1.1$ and $P_{laser} = 0.76$ TW. Note that the power is greater than the critical power for relativistic self-focusing $P > P_c = 17.4\omega_0^2/\omega_p^2$, so that self-focusing should occur during the interaction. The simulation box is a window moving at the laser linear group velocity $v_g = 0.97c$, with Lorentz factor $\gamma_g = 4.1$. The box is composed of 1500x200 cells with 220 particles per cell. The longitudinal cell size is 0.125 c/ω_0 and the radial cell size is 0.628 c/ω_0.

We first simulated the propagation of an unchirped pulse. Figure 1 shows snapshots of the laser field $|E/E_0|^2$ (where $E_0 = m_e c\omega_0/e$), the on-axis laser spectrum and phase as well as the corresponding wakefield excitation, at different positions in the plasma. As can be seen in the figure, the pulse first undergoes transverse self-focusing, see panels 1(a) and 1(d), along with strong spectral broadening and redshifting due to nonlinear effects and plasma wave excitation, see panels 1(c) and 1(f). In addition, the curvature of the spectral phase $\phi(\omega)$ (green curves) indicates that the pulse has a negative chirp as soon as it reaches the plateau at $x = 65\,\mu$m, see panel 1(c). This is evidence that GVD is acting from the start and that it is overwhelming the frequency changes caused by nonlinear effects: even though the plasma wave redshifts the front of the pulse, red wavelengths quickly slip backward because of GVD and blue wavelengths re-

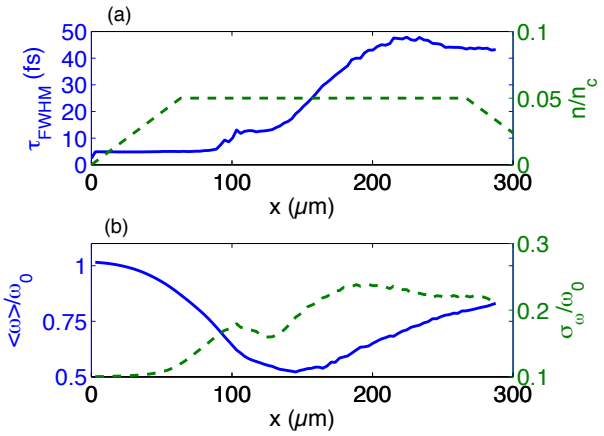

FIG. 2: a) Dashed green line: electronic density profile. Full blue line: on-axis FWHM pulse duration as a function of propagation . b) Full blue line: on-axis average laser frequency. Dashed green line: r.m.s. laser spectral width as a function of propagation.

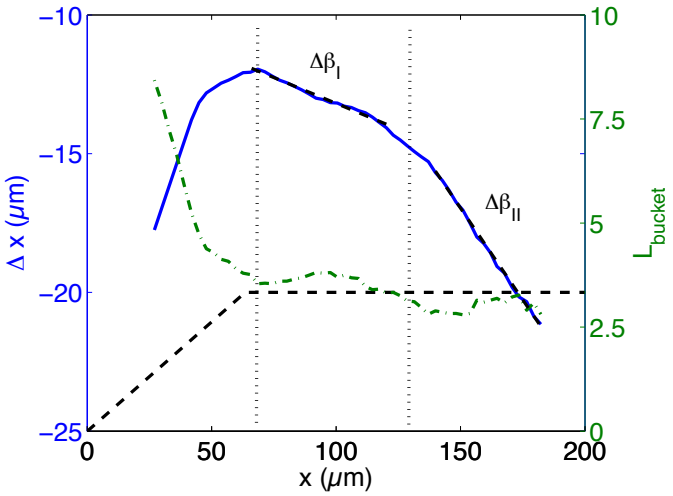

FIG. 3: Full blue line: evolution of the position of the back of the first plasma bucket (Δx) relative to the front of the moving window. Dashed green line: longitudinal size of the first plasma bucket. Black dashed line: electron density profile.

main at the front. This scenario is even more accentuated later in the propagation: in panel 1(g) at $x = 140\,\mu$m, the pulse has stretched by an important amount and the red wavelengths are clearly at the back of the pulse, while the blue part at the front of the pulse is diffracting away. In addition, a giant redshifting has occurred and the pulse central frequency is now $\omega_0/2$. An important consequence of these effects is that the pulse centroid is slipping backward which causes the plasma wakefield to slow down by an important amount. Comparison of panel 1(e) and 1(h) clearly shows the wakefield deceleration which is also accompanied by trapping of electrons. Finally, at $x = 180\,\mu$m, the laser pulse cannot sustain self-focusing: it diffracts away while GVD is continuously stretching the pulse duration.

This behavior is even clearer when looking at the various on-axis physical quantities in Fig. 2. Fig 2a) shows the evolution of the on-axis FWHM duration of the pulse as a function of position in the plasma. Fig. 2b) shows the evolution of the r.m.s. spectral width σ_ω/ω_0 as well as the average frequency $\langle\omega\rangle/\omega_0$ of the distribution in Fourier space. In Fig. 2a, one can see that the FWHM duration does not change while the pulse is propagating in the ramp: nonlinear effects are still small and linear dispersion in the ramp can be neglected, as predicted by the linear theory presented in the previous section. As the pulse enters the high density plateau, $x > 70\,\mu$m nonlinear effects become more important: Fig. 2b) shows large spectral broadening (the bandwidth is multiplied by 2) and large redshifting of the whole spectrum. In the middle of the plateau, $x \simeq 150\,\mu$m, the average laser frequency has been divided by a factor of 2. This complex spectral dynamics explains why the laser pulse duration experiences a lengthening at a rate much faster than $(1 + x^2/L_p^2)^{1/2}$, with $L_p = 111\,\mu$m as computed in the previous section. In fact, taking into account that after propagation in the plateau, the pulse central frequency shifts toward $\omega_0/2$, Eq. 3 gives $L_p(\omega_0/2) = 15\,\mu$m. In consequence, linear dispersion theory predicts that the redshifted pulse should lengthen by a factor of 6.5 after a $100\,\mu$m propagation, which is close to the behavior of Fig. 2a.

The striking feature of these results is that the pulse does not undergo self-compression, as observed in experiments and simulations at lower densities and using longer pulses [29, 31, 32]. On the contrary the laser pulse acquires a negative chirp and stretches as it propagates. Thus dispersion becomes a key ingredient of the interaction and even dominates over nonlinear effects. The importance of dispersion is enhanced by the fact that (i) nonlinear effects broaden the bandwidth even more, (ii) dispersion is more important for the redshifted radiation, (iii) even after self-focusing has occurred, $a_0 < 2$ and the plasma wake is not nonlinear enough to trap the laser radiation and compress it. In fact, in this regime, it is clear that the sustained propagation of a self-focused and self-compressed laser pulse is not possible.

However, an important side effect of these phenomena is that the laser pulse group velocity slows down considerably as the laser spectrum becomes redshifted, resulting in a concomitant deceleration of the wakefield. The deceleration of the wakefield, already visible in Fig. 1, is quantitatively analyzed in Fig. 3. Fig. 3 shows the evolution of the plasma bucket longitudinal size (dashed green line) as a function of propagation. The figure also shows the position of the back of the first plasma bucket Δx relative to the front of the moving window. In the gradient, i.e. $x < 60\,\mu$m, the plasma bucket shortens and

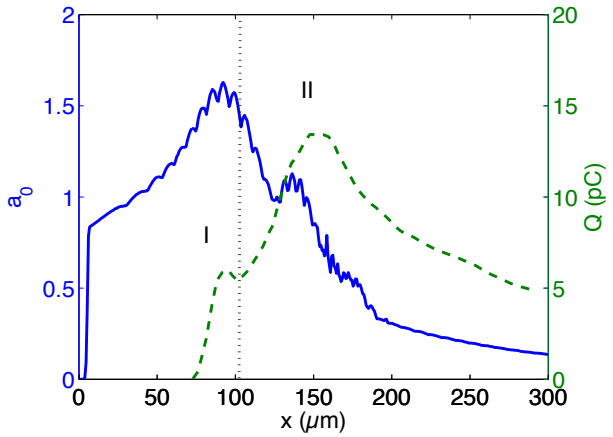

FIG. 4: Full blue line: evolution of the normalized vector potential a_0 during propagation. Dashed green line: evolution of the beam charge for electrons with $\gamma > 6$ and located within 2.5 μm of the x-axis.

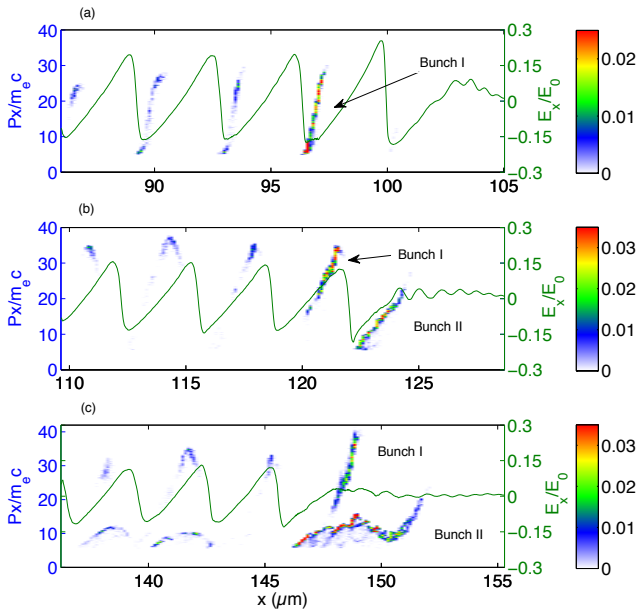

FIG. 5: Electron density in phase space (x, p_x/mc) at various positions in the plasma. Full green line: on-axis plasma longitudinal electric field.

moves forward, as expected from the rising electron density. The behavior in the plateau is more surprising: in the region $70-100\,\mu$m the bucket slightly expands while it slightly contracts for $x > 100\,\mu$m. The slight expansion of the bucket size is due to the fact that the wakefield nonlinearity increases as the laser pulse self-focuses in the region $70-100\,\mu$m. However, the general trend is that the bucket size does not evolve a lot in the plateau, it varies only slightly around $3.5\,\mu$m. A much larger effect is the deceleration of the wake: the wakefield slips backward by about $10\,\mu$m in only $100\,\mu$m of propagation. This deceleration occurs in two stages: for $x = 70-110\,\mu$m, the phase velocity is $v_{p1}/c = \beta_{p1} = \beta_g - \Delta\beta_1 = 0.9$, corresponding to $\gamma_{p1} = 2.3$. For $x > 110\,\mu$m, as the laser gets massively redshifted, the wake slows down even more, as indicated by the change of slope in Fig. 3. The wake phase velocity then decreases to $\beta_{p2} = 0.727$, i.e. $\gamma_{p2} = 1.45$. Clearly, at this point, the wakefield has a sub-relativistic phase velocity. Note that the group velocity of the redshifted laser pulse with central wavelength $v_g(\omega_0/2) = 0.89$, i.e. $\gamma_g = 2.2$. Thus, it seems that the wake is even slower than the linear group velocity of the red shifted laser pulse $\gamma_{p2} < \gamma_g(\omega_0/2)$, possibly because of etching effects [10, 36]. This effect is very fortunate because it considerably lowers the threshold for self-injection even though the wakefield amplitude and a_0 are modest.

We now turn to electron trapping and acceleration in the nonlinear wake. In the simulation, we observe that a large amount of electrons are trapped and further accelerated. To illustrate this, the evolution of the number of electrons with a gamma factor $\gamma > 6$ (i.e. an energy $\epsilon > 3$ MeV) is represented in Fig. 4. The evolution of the maximum of the normalized vector potential is also shown on the same graph. We observe that trapping occurs in two stages: a first bunch is trapped in the region $x = 75 - 100\,\mu$m which corresponds to the maximum of laser intensity, $a_0 = 1.6$. Here, the wakefield amplitude is high because the laser is at its peak intensity, which facilitates trapping. Most importantly, trapping is also enhanced by the slowdown of the back of the wake. The slowdown has two main causes: (i) the elongation of the plasma bucket which facilitate trapping [37] (ii) the overall slowdown of the plasma wake at $\gamma_{p1} = 2.3$. In the second trapping stage, the injection mechanism is different because the laser amplitude is modest ($a_0 \simeq 1.1$) and the plasma buckets are now shrinking instead of elongating. Yet, the second trapping stage, which occurs in the region $x = 130 - 150\,\mu$m, injects twice as much charge, up to $\simeq 15$ pC. This is because this region also corresponds to the maximum redshift of the laser pulse, i.e. the region where the laser pulse and the wakefield are the slowest: $\gamma_{p2} = 1.45$. Therefore, we interpret this enhanced trapping by the large deceleration of the plasma wakefield induced by the laser pulse giant redshifting.

The dynamics of trapping and acceleration is illustrated through phase space plots in Fig. 5. The electron density is represented in the (x, p_x/mc) phase space. Panel (a) shows that at $x = 100\,\mu$m, corresponding to the first injection stage, a large fraction of charge has been trapped in the second plasma bucket (bunch I in Fig. 5a). The charge in this bunch reaches 3.7 pC, i.e. about 70 % of the total injected charge. In panel (b), at $x = 120\,\mu$m, the second injected stage has started and bunch II is injected in the first plasma bucket. As explained earlier, bunch II is injected because of the strong wakefield deceleration. Note that at this point,

bunch I has completely dephased and enters a decelerating phase. Finally, at $x = 150\,\mu$m, both bunches have outrun the wakefield and are now propagating ballistically. Note that bunch II has energies in the 5 MeV range whereas bunch I has electrons in excess of 10 MeV. This can simply be explained by dephasing: bunch II is trapped in a slower wakefield in which dephasing occurs much quicker, thus the energy gain is lower. Simple estimates can be obtained by computing the maximum electron energy gain in a linear plasma wave with Lorentz factor γ_p: $\Delta\gamma = 4\gamma_p^2(E/E_0)\omega_0/\omega_p$. Thus, the ratio of energy gain between bunch I and bunch II should scale as $(\gamma_{p1}/\gamma_{p2})^2 \simeq 2.5$, which is in agreement with the PIC simulation, see Fig. 5c. Note that the injection of bunch II, which occurs in the sub-relativistic wakefield, accelerates electrons toward 5 MeV, a range better suited for application to electron diffraction [17–19].

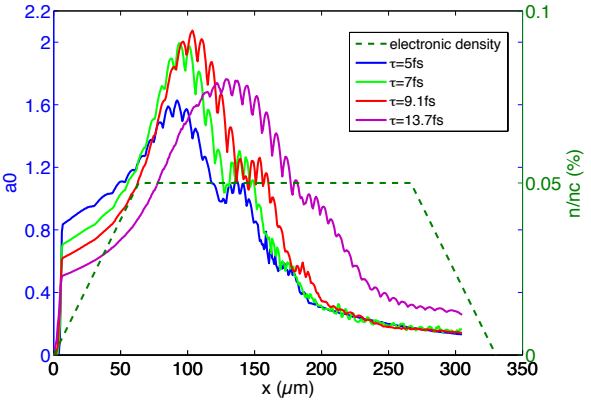

FIG. 6: Evolution of the normalized vector potential a_0 during propagation for various chirped pulses. Full blue line: unchirped pulse. Full green, red and purple lines are for pulses positively chirped to 7 fs, 9 fs and 13.7 fs. Green dashed curve: electron density profile.

IV. INFLUENCE OF THE CHIRP ON PROPAGATION AND ELECTRON TRAPPING

Since dispersion is such an important ingredient of the interaction, it is natural to think of introducing some chirp in the laser pulse in order to pre-compensate linear dispersion and attempt to control the pulse propagation. The use of chirped pulses in relativistic laser interaction has been explored in previous work, first for studying or trying to enhance the self-modulation instability [38, 39]. It was found that the sign of the chirped has little influence on the growth of instabilities. In Ref. [39], chirped pulses could cause an increase of the trapped charge but it was found that the modification of the pulse envelope due to high order dispersion terms was the reason why trapping increased and not really the chirp itself. More recent work has focused on using chirped pulses in the blow out regime [40, 41]. Large effect of the chirp was only found when comparing a unchirped pulse and a chirped pulse with the same duration and a_0, i.e. with different bandwidths. In other words, simply chirping a laser pulse with a given bandwidth has usually little effect on the interaction other than lengthening the pulse duration and lowering a_0. In Ref. [40], the authors use a negative chirp and a broad bandwidth to slow down laser pulse evolution caused by nonlinear effects: the idea is that a negative chirp has a blue front which gets redshifted, resulting in a slower spectral broadening and overall redshifting. On the contrary, a pulse with a positive chirp will evolve faster because its red front gets even more redshifted by the plasma [41]. In this context, we have decided to explore interaction with positively chirped laser pulses for two reasons (i) pre-compensate the negative dispersion of the plasma (ii) enhance the effects of plasma nonlinearities in order to increase electron trapping.

In the simulations, the chirp is included in the phase of the laser field as $\phi = \omega t + bt^2$ where the chirp parameter b is defined as

$$b = \pm\frac{1}{4\Delta t^2}\sqrt{\frac{\Delta t^2}{\Delta t_0^2} - 1} \qquad (4)$$

Where Δt_0 and Δt are the r.m.s. transform limited and chirped duration respectively. The $\pm$ sign stands for positive or negative chirp respectively. We have studied the effect of a positive chirp for a 5 fs transform limited pulse chirped to FWHM duration of τ= 7 fs, 9 fs and 13.7 fs. The stricking effect of the positive chirp is that it permits to tune the laser pulse temporal focus in the plasma and to enhance the amplitude of the laser field. This is illustrated in fig. 6 which represents the evolution of the normalized vector potential a_0 during propagation. The figure clearly shows that when the pulse is stretched to 7 fs and 9 fs, the laser field reaches $a_0 = 2$ which is higher than the unchirped case for which $a_0 < 1.6$. In addition, it is also clear that the position of maximum a_0 is shifting with the chirp. This increase of the laser field amplitude, which is due to the effect of GVD, is quite original and has not been observed for longer pulses and smaller plasma densities.

In order to confirm that the increase of a_0 is a purely temporal effect, we have plotted in fig. 7 the on-axis laser temporal profile at the maxima of a_0 for the different cases. Pulses initially chirped to 7 fs and 9 fs, see panels 7c) and 7e), have turned into a single cycle field whereas the initially unchirped pulse is longer and has acquired a negative chirp, see panel a). This clearly illustrates that dispersion compensation using positive chirp works. In the case of a pulse initially chirped to 13.7 fs, the positive chirp was initially too large and the pulse does not recompress in the plasma: it still has a positive chirp at the maximum of self-focusing resulting in a smaller value of a_0, see panels g) and h). Note that for negative

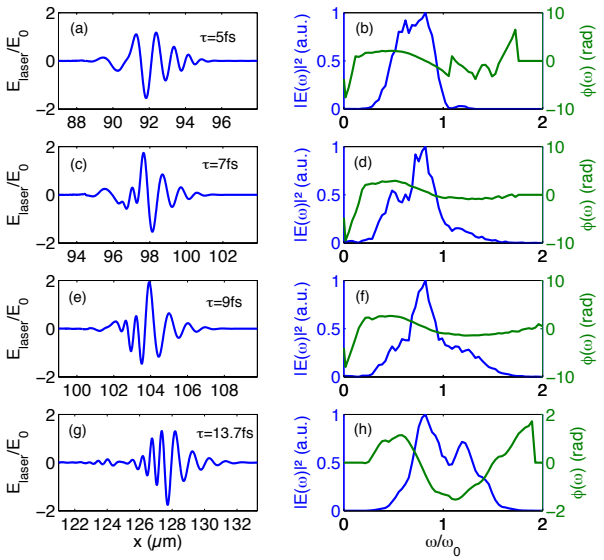

FIG. 7: a) - c) - e) - g) On-axis laser field E_{laser}/E_0 at the maxima of a_0 for various initial chirps. b) - d) - f)- h) corresponding on-axis laser spectrum (full blue line) and spectral phase (full green line).

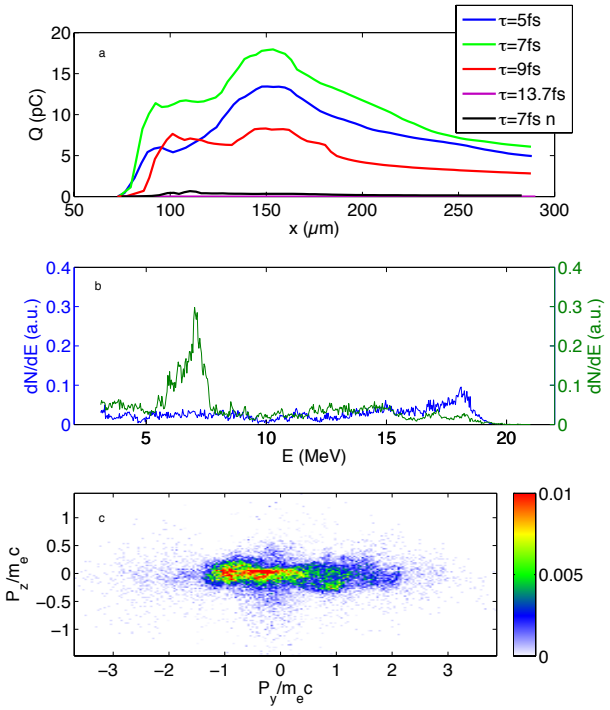

FIG. 8: Effect of the chirp on the trapped charge ($\gamma > 6$). Blue line: the unchirped pulse, the green, red and purple lines: positive chirps with 7 fs, 9 fs and 13.7 fs; the black line is for a pulse negatively chirped to 7 fs. b) Electron energy distribution for the case of an unchirped pulse. Blue line: spectrum at $x = 123\,\mu$m; green line: spectrum at $x = 137\,\mu$m. c) Electron density in transverse phase space for the case of an unchirped pulse.

chirps (not shown here), the pulse duration never shortens and self-focusing is less efficient. Therefore negative chirps, as expected, are not adapted for enhancing the interaction. Finally our analysis also indicates that the transverse dynamics is similar for the various chirps: the transverse laser size does not depend on the chirp. Therefore one can conclude that the field dynamics is mostly governed by longitudinal effects.

Fig. 7 b),d),f) and h) also shows the laser spectra at the maxima of a_0. The spectral shapes are very different according to the initial chirps, indicating the importance of the chirp in the nonlinear pulse evolution. The data shows that the shorter the pulse, the more red shift. On the other hand, the longer chirped pulses experience a more symmetric spectral broadening with more blue shift. This can be explained simply: the shorter pulses reside more at the front of the plasma bucket and thus experience a negative gradient of the index of refraction, resulting mostly in red shifting. The longer chirped pulses, on the other hand, also experience the back of the bucket, where the index of refraction has a positive gradient, leading to blue shifting at the laser trail, and eventually to a more symmetric spectral broadening.

These results indicate that the chirp can be used as a tuning knob for the interaction. It permits to compensate the plasma negative GVD, adjust the temporal focus of the laser pulse and increase the laser field amplitude. The results in fig. 8 show that the chirp can also be used to optimize the injected charge. Fig. 8a) represents the trapped charge during propagation and for various chirps. When using a 7 fs chirped pulse, the injected charge in the first bunch can be multiplied by two compared to the unchirped case. Similarly, the overall beam charge, including first and second injection, can be increased by 30%. The figure also shows that when the positive chirp is too high (purple line), no trapping occurs. Similarly, no trapping occurs for a negatively chirped pulse (black line).

Thus, the effect of the positive chirp is mainly to increase injection in the first bucket, in conjunction with the enhancement of a_0. On the other hand, injection in the second bucket is optimized for the shortest pulse. Fig. 8b) shows the electron energy distribution in the case of an unchirped laser pulse, i.e. the charge is optimized for the second injection. The blue curve represents the energy distribution of the first bunch at $x = 123\,\mu$m. Energies extend to 20 MeV but the distribution is rather flat. At $x = 137\,\mu$m, the second bunch has been injected and it has a peaked energy distribution at 7 MeV, with a relative energy spread $\Delta E/E = 12.6\%$. The charge in the peak is $\simeq 8.5$ pC. Fig. 8c) shows the electron density in transverse phase space showing that the beam is well

defined. Its divergence is larger in the laser polarization direction because of the interaction with the transverse laser field as the bunch is rapidly dephasing. The FWHM beam divergence is 12 (90) mrad in the direction perpendicular (parallel) to the laser polarization. The normalized emittance obtained from the usable phase space density (i.e. containing 50% of the charge) is $\epsilon_n = 6 \times 10^{-3}$ mm.mrad (0.2 mm.mrad) in the direction perpendicular (parallel) to the polarization direction.

While the beam energy is in a range suitable for application to UED, it would be necessary to reduce the energy spread by (i) using another injection scheme [20] or (ii) using an energy filter, as in Ref. [42]. For instance, limiting the relative energy spread to 2% would keep the beam charge to a relatively high value of 1.1 pC. The electron bunch duration of this filtered beam could be as short as $\simeq$ 14 fs. Future work will focus on the design of an actual beamline for filtering and transporting the electron beam while preserving the bunch duration.

V. CONCLUSION

To conclude, we have performed PIC simulation of the interaction of 5 fs few-cycle, few millijoule laser pulses with underdense plasmas at resonant density ($n/n_c = 5\%$). We found that in this particular regime, dispersion cannot be neglected and plays an important role in the interaction. Giant redshifting of the laser pulse leads to the excitation of sub-relativistic wakefields which can trap copious amounts of electrons in the 5-10 MeV range. While experiments in this particular regime still needs to be developed, the electron bunches produced in this manner could become useful for ultrafast electron diffraction, provided that transport and filtering improve the energy spread. Our analysis also shows that in this dispersion dominated regime, the chirp can be used as an extra knob to tune the interaction, adjust the position of the temporal focus, increase the laser amplitude, or improve the amount of accelerated charge.

Appendix A: Plasma dispersion for arbitrarily broadband pulses

Here, we present a brief theory for linear dispersion which is valid for arbitrarily broadband pulses. In the linear regime, i.e. if the normalized potential vector $a_0 \ll 1$ and the perturbation of the electronic density $\delta n/n \ll 1$, the refractive index can be written $\eta = 1 - \omega_p^2/2\omega^2$ for tenuous plasmas. In order to estimate the effect of dispersion, we calculate the duration of the pulse propagating in the plasma by evaluating the variance of the intensity distribution $\Delta t^2(x) = \langle t^2 - \langle\, t\rangle^2\rangle$, where $\langle\,\rangle$ represents the average over the intensity distribution. Let $E(\omega) = |E(\omega)| \exp[i\phi(\omega)]$ be the laser electric field in the frequency domain and $\phi(\omega)$ the spectral phase. Using the properties of Fourier Transform, one can write

$$\begin{aligned}\langle t^2\rangle &= A\int_{-\infty}^{+\infty} t^2|E(t)|^2\,\mathrm{d}t = A\int_{-\infty}^{+\infty}\left|\frac{d\,E(\omega)}{d\,\omega}\right|^2\frac{\mathrm{d}\omega}{2\pi}\\ &= \int_{-\infty}^{+\infty}\frac{d|E(\omega)|}{d\omega}^2\frac{\mathrm{d}\omega}{2\pi} + \int_{-\infty}^{+\infty}\left(\frac{d\phi}{d\omega}\right)^2|E(\omega)|^2\frac{\mathrm{d}\omega}{2\pi}\\ &= \langle t^2\rangle_{\phi=0} + \left\langle\left(\frac{d\phi}{d\omega}\right)^2\right\rangle\end{aligned}$$

where A is a normalization factor. Obviously, one can identify the transform limited pulse duration Δt_0 as $\Delta t_0 = \langle t^2\rangle_{\phi=0}$. We apply a similar analysis for calculating $\langle t\rangle$ in order to finally express the r.m.s. pulse duration $\Delta t(x) = \sqrt{\Delta t_0^2 + \Delta\tau_g^2(x)}$ where $\tau_g = d\phi/d\omega$ is the group delay which we compute from the spectral phase $\phi = \frac{\omega}{c}\int_0^x \eta\,\mathrm{d}x$. The evolution of the pulse duration can then be rewritten in a more convenient way: $\Delta t(x) = \Delta t_0\sqrt{1 + x^2/L_p^2}$ with

$$L_p = \frac{2c\Delta t_0}{\omega_p^2}\left\langle\left(\frac{1}{\omega^2} - \left\langle\frac{1}{\omega^2}\right\rangle\right)^2\right\rangle^{-1/2} \tag{A1}$$

This expression is valid for arbitrary broadband pulses and includes only second order dispersion.

Acknowledgments

This work was funded by the European Research Council under Contract No. 306708, ERC Starting Grant FEMTOELEC.

[1] T. Brabec and F. Krausz, Rev. Mod. Phys. **72**, 545 (2000).

[2] F. Krausz and M. Ivanov, Rev. Mod. Phys. **81**, 163 (2009).

[3] S. Bohman, A. Suda, T. Kanai, S. Yamaguchi, and K. Midorikawa, Opt. Lett. **35**, 1887 (2010).

[4] X. Chen, A. Malvache, A. Ricci, A. Jullien, and R. Lopez-Martens, Laser Physics **21**, 198 (2011).

[5] A. G. Mordovanakis, J. Easter, N. Naumova, K. Popov, P.-E. Masson-Laborde, B. Hou, I. Sokolov, G. Mourou, I. V. Glazyrin, W. Rozmus, et al., Phys. Rev. Lett. **103**, 235001 (2009).

[6] A. Borot, A. Malvache, X. Chen, D. Douillet, G. Iaquianiello, T. Lefrou, P. Audebert, J.-P. Geindre, G. Mourou,

F. Quéré, et al., Opt. Lett. **36**, 1461 (2011).
[7] A. Borot, A. Malvache, X. Chen, A. Jullien, J.-P. Geindre, P. Audebert, G. Mourou, F. Quéré, and R. Lopez-Martens, Nat. Phys. **8**, 416 (2012).
[8] J. Faure, Y. Glinec, A. Pukhov, S. Kiselev, S. Gordienko, E. Lefebvre, J.-P. Rousseau, F. Burgy, and V. Malka, Nature **431**, 541 (2004).
[9] W. P. Leemans, B. Nagler, A. J. Gonsalves, C. Tòth, K. Nakamura, C. G. R. Geddes, E. Esarey, C. B. Schroeder, and S. M. Hooker, Nat. Phys. **2**, 696 (2006).
[10] W. Lu, M. Tzoufras, C. Joshi, F. S. Tsung, W. B. Mori, J. Vieira, R. A. Fonseca, and L. O. Silva, Phys. Rev. ST Accel. Beams **10**, 061301 (2007).
[11] S. Gordienko and A. Pukhov, Phys. Plasmas **12**, 043109 (2005).
[12] G. Sciaini and R. J. D. Miller, Rep. Prog. Phys. **74**, 096101 (2011).
[13] O. Lundh, J. Lim, C. Rechatin, L. Ammoura, A. Ben-Ismail, X. Davoine, G. Gallot, J.-P. Goddet, E. Lefebvre, V. Malka, et al., Nat. Phys. **7**, 219 (2011).
[14] Z.-H. He, B. Hou, J. A. Nees, J. H. Easter, J. Faure, K. Krushelnick, and A. G. R. Thomas, New Journal of Physics **15**, 053016 (2013).
[15] Z.-H. He, A. G. R. Thomas, B. Beaurepaire, J. A. Nees, B. Hou, V. Malka, K. Krushelnick, and J. Faure, Appl. Phys. Lett. **102**, 064104 (2013).
[16] K. Schmid, L. Veisz, F. Tavella, S. Benavides, R. Tautz, D. Herrmann, A. Buck, B. Hidding, A. Marcinkevicius, U. Schramm, et al., Phys. Rev. Lett. **102**, 124801 (2009).
[17] J. B. Hastings, F. M. Rudakov, D. H. Dowell, J. F. Schmerge, J. D. Cardoza, J. M. Castro, S. M. Gierman, H. Loos, and P. M. Weber, Appl. Phys. Lett. **89**, 184109 (2006).
[18] Y. Murooka, N. Naruse, S. Sakakihara, M. Ishimaru, J. Yang, and K. Tanimura, Appl. Phys. Lett. **98**, 251903 (2011).
[19] P. Musumeci, J. T. Moody, C. M. Scoby, M. S. Gutierrez, H. A. Bender, and N. S. Wilcox, Rev. Sci. Instrum. **81**, 013306 (2010).
[20] A. F. Lifschitz and V. Malka, New J. Phys. **14**, 053045 (2012).
[21] W. B. Mori, IEEE J. Quant. Elec. **33**, 1942 (1997).
[22] G. Sun, E. Ott, Y. C. Lee, and P. Guzdar, Phys. Fluids **30**, 526 (1987).
[23] A. B. Borisov, A. V. Borovski, O. B. Shiryaev, V. V. Korobkib, A. M. Prokhoraov, T. S. Luk, K. Boyer, and C. K. Rhodes, Phys. Rev. A **45**, 5830 (1992).
[24] N. E. Andreev, L. M. Gorbunov, V. I. Kirsanov, A. A. Pogosova, and R. R. Ramazashvili, JETP Lett **55**, 571 (1992).
[25] P. Sprangle and E. Esarey, Phys. Fluids B **4**, 2241 (1992).
[26] T. M. Antonsen, Jr. and P. Mora, Phys. Rev. Lett. **69**, 2204 (1992).
[27] E. Esarey, C. B. Schroeder, B. A. Shadwick, J. S. Wurtele, and W. P. Leemans, Phys. Rev. Lett. **84**, 3081 (2000).
[28] J. Vieira, F. Fiúza, L. O. Silva, M. Tzoufras, and W. B. Mori, New Journal of Physics **12**, 045025 (2010).
[29] C. Ren, B. J. Duda, R. G. Hemker, W. B. Mori, T. Katsouleas, T. M. Antonsen, Jr., and P. Mora, Phys. Rev. E **63**, 26411 (2001).
[30] F. S. Tsung, C. Ren, L. O. Silva, W. B. Mori, and T. Katsouleas, Proc. Nat. Acad. Science **99**, 29 (2002).
[31] J. Faure, Y. Glinec, J. J. Santos, F. Ewald, J.-P. Rousseau, S. Kiselev, A. Pukhov, T. Hosokai, and V. Malka, Phys. Rev. Lett. **95**, 205003 (2005).
[32] J. Schreiber, C. Bellei, S. P. D. Mangles, C. Kamperidis, S. Kneip, S. R. Nagel, C. A. J. Palmer, P. P. Rajeev, M. J. V. Streeter, and Z. Najmudin, Phys. Rev. Lett. **105**, 235003 (2010).
[33] L. Silva and J. T. Mendonça, Phys. Rev. E **57**, 3423 (1998).
[34] C. D. Murphy, R. Trines, J. Vieira, A. J. W. Reitsma, R. Bingham, J. L. Collier, E. J. Divall, P. S. Foster, C. J. Hooker, A. J. Langley, et al., Phys. Plasmas **13**, 033108 (2006).
[35] A. Lifschitz, X. Davoine, E. Lefebvre, J. Faure, C. Rechatin, and V. Malka, Journal of Computational Physics **228**, 1803 (2009).
[36] C. D. Decker and W. B. Mori, Phys. Rev. Lett. **72**, 490 (1994).
[37] S. Y. Kalmykov, A. Beck, S. A. Yi, V. N. Khudik, M. C. Downer, E. Lefebvre, B. A. Shadwick, and D. P. Umstadter, Physics of Plasmas **18**, 056704 (2011).
[38] J. Faure, J.-R. Marquès, V. Malka, F. Amiranoff, Z. Najmudin, B. Walton, J.-P. Rousseau, S. Ranc, A. Solodov, and P. Mora, Phys. Rev. E **63**, 654 (2001).
[39] W. P. Leemans, C. G. R. Geddes, J. Faure, C. Tóth, J. van Tilborg, C. B. Schroeder, E. Esarey, G. Fubiani, D. Auerbach, B. Marcelis, et al., Phys. Rev. Lett. **91**, 074802 (2003).
[40] S. Y. Kalmykov, A. Beck, X. Davoine, E. Lefebvre, and B. A. Shadwick, New Journal of Physics **14**, 033025 (2012).
[41] V. B. Pathak, J. Vieira, R. A. Fonseca, and L. O. Silva, New Journal of Physics **14**, 023057 (2012).
[42] S. Tokita, M. Hashida, S. Inoue, T. Nishoji, K. Otani, and S. Sakabe, Phys. Rev. Lett. **105**, 215004 (2010).